Proceedings of the ASME 2013 11th Fuel Cell Science, Engineering and Technology Conference
FuelCell2013
July 14-19, 2013, Minneapolis, MN, USA

FuelCell2013-18132

IN-PLANE MICROSTRUCTURE OF GAS DIFFUSION LAYERS WITH DIFFERENT PROPERTIES FOR PEFC

Mehdi Mortazavi
Multiscale Transport Process Laboratory
Mechanical Engineering-Engineering Mechanics
Michigan Technological University
Houghton, Michigan 49931
Email: mortazav@mtu.edu

Kazuya Tajiri*
Mechanical Engineering-Engineering Mechanics
Michigan Technological University
Houghton, Michigan, 49931
Email: ktajiri@mtu.edu

ABSTRACT

Gas diffusion layer (GDL) is undoubtedly one of the most complicated components used in a polymer electrolyte fuel cell (PEFC) in terms of liquid and gas transport phenomena. An appropriate fuel cell design seeks a fundamental study of this tortuous porous component. Currently, porosity and gas permeability have been known as some of the key parameters affecting liquid and gas transport through GDL. Although these are dominant parameters defining mass transport through porous layers, there are still many other factors affecting transport phenomena as well as overall cell performance. In this work, microstructural properties of Toray carbon papers with different thicknesses and for polytetrafluoroethylene (PTFE) treated and untreated cases have been studied based on scanning electron microscopy (SEM) image analysis. Water droplet contact angle as a dominant macroscale property as well as mean pore diameter, pore diameter distribution, and pore roundness distribution as important microscale properties have been studied. It was observed that the mean pore diameter of Toray carbon paper does not change with its thickness and PTFE content. Mean pore diameter for Toray carbon papers was calculated to be around 26μm regardless of their thicknesses and PTFE content. It was also observed that droplet contact angle on GDL surface does not vary with GDL thickness. The average contact angle for 10 wt.% PTFE treated GDLs of different thicknesses was measured about 150°. Finally, the heterogeneous in-plane PTFE distribution on the GDL surface was observed to have no effect on mean pore diameter of GDLs.

INTRODUCTION

Although Polymer electrolyte fuel cell (PEFC) has gained lots of consideration as a clean type of energy system, there are still some technical challenges needed to be solved before this type of energy system can be commercially released. Among these challenges, one can refer to water management in PEFC. During the operation of a PEFC, oxygen is reduced in the cathode and is accompanied by water production. Some amount of this produced water may fill open pores of gas diffusion layer (GDL). GDL is macro-porous layer with multifunction purposes such as providing a uniform transport of reactants to the catalyst layer, removing excess water from the membrane by providing pathways of water to the gas channel, mechanically protecting the membrane as a fragile thin layer, and providing electrical conductivity between the electrodes and the current collectors. An appropriate design of GDL has been reported to have a significant contribution on proper water balance within the cell [1–4].

For a continues transport of reactants to the catalyst layer and transport of excess water to the gas channel, GDL pores should be free from accumulated liquid water. Excess water accumulated within the GDL pores and gas flow channels blocks reactants flow to catalyst layer and finally results in oxidant starvation and performance loss. Liquid water accumulated within the GDL pores, emerges from the GDL surface in form of

*Address all correspondence to this author.

droplet.

Liquid water transport mechanism on GDL surface is a function of superficial gas velocity, defined as the bulk velocity of gas flowing within the channel cross sectional area, and droplet emergence rate [5]. While for high superficial gas velocities the drag force from shear gas flow can easily detach water droplet from the GDL surface, moderate or low superficial gas velocity is not capable of detaching the droplet directly from the GDL surface. Instead, droplet grows in size until it touches the gas channel walls and spreads over them. In such cases, capillary flow drains liquid water through the corners, forming annular film flow. For high liquid water production rate and/or low superficial gas velocity, water film will not be drained properly and the channel will be clogged as the liquid film grows.

Water transport mechanisms within the GDL are quite different from liquid water transport on GDL surface and can be categorized into diffusion, pressure driven hydraulic permeation and evaporation [6]. Liquid water behavior on GDL surface can be studied by simple optical visualization techniques [5, 7–10] while water behavior within the GDL cannot be monitored easily. Some of the techniques used for studying water behavior within the GDL are X-ray and neutron radiography [11] since both X-ray and neutron beams are capable of penetrating through the GDL. However each of these techniques has their own drawbacks. For instance, expensive hardware of neutron imaging requires challenging calibration to ensure a reliable data acquisition [12].

It is a common practice to treat GDLs with some hydrophobic media such as polytetrafluoroethylene (PTFE) to enhance gas transport as well as liquid water transport through the pores when the cell is operating at flooding condition [13]. Park et al. [14] tested GDLs with different amount of PTFE and obtained I-V curves of a single cell working at different level of relative humidities. They concluded that among different water transport mechanisms within the GDL, evaporation and shear force are more dominant than capillary force and attributed that to relatively large pore diameters of GDLs compared to microporous layer and catalyst layer. Pasaogullari and Wang [15] used one-dimensional analytical solution and concluded that liquid water transport within the GDL is controlled by capillary forces arising from the gradient in phase saturation. Nam and Kaviany [16] studied water transport within the GDL by developing a capillary pressure model and hypothesized that water is distributed as an "upside-down tree" capillary network. Litster et al. [17] followed a fluorescence microscopy technique and visualized liquid water transport in GDL. They suggested that water transport within the GDL is mostly dominated by fingering and channeling in such a way that as a breakthrough path within the GDL forms, liquid water existing in other pathes recede back and find their way through the newly formed breakthrough path. The hereby illustrated literature review highlights different and sometimes opposite hypothesises made regarding liquid water transport through the GDL.

Water transport through and on the surface of GDL can be characterized by two independent parameters of GDL microstructure and pore surface wettability [3]. GDL pore diameter, for instance, was known to directly affect the water vapor pressure at which condensation occurs according to Kelvin equation [18] and for a vapor pressures below saturation pressure, water vapor starts condensing in a pore smaller than critical pore diameter [1]. In this article, GDL microstructure has been studied by processing SEM images taken from untreated and treated GDLs with different thicknesses. SEM images of Toray carbon papers with different thicknesses have been analyzed to obtain microstructural properties such as mean pore diameter, pore diameter distribution, and pore roundness. Since all of the GDLs used in this study have the same production procedure, it is expected to obtain similar microstructure for all the samples used. Air permeability, on the other hand, is a property that can be used for comparing microstructure of porous materials [19]. Very close air permeability of the GDL samples used in this study as listed in Table 1 can be an indication of similar microstructure of Toray carbon papers of different thicknesses [19].

EXPERIMENTAL

Toray carbon papers with different thicknesses were used as GDL in this study. GDLs with manufacturer specified thicknesses of 110μm, 190μm, 280μm, and 370μm have been used. For each thickness, untreated and 10 wt.% PTFE treated papers were tested for microstructural analysis. For PTFE treating the GDL samples, Toray carbon papers were loaded with PTFE based on the procedure given in [20]. This procedure is described as follows. The substrates were first dipped in PTFE emulsion (60 wt.% dispersion in H_2O, ALDRICH) for ten hours and then they were put in furnace at 120°C for one hour to make them dry. In order to make a uniform distribution of the PTFE within the GDL substrates, they were sintered at 360°C for one hour. Static contact angles of liquid water droplet on GDL samples with different PTFE contents were measured using a house-made setup designed and made specifically for this purpose [21] with procedure and theory given in [22]. Ten droplets with diameters within the range of 1mm – 3mm were dropped on GDL surfaces and mean contact angles were considered. Table 1 lists measured and calculated physical properties of the samples used in this study. GDL thicknesses were measured using an electronic micrometer (Mitsutoyo, Japan). The measured thicknesses were slightly different from the thicknesses specified by the manufacturer. However, the manufacturer specified thicknesses are used for the remainder of the paper.

The surface morphology of GDL samples were scanned using a JEOL JSM-6400LV scanning electron microscope (SEM) at 20keV and 250× magnification. For each sample, three random locations were chosen and images were obtained. SEM

images were analyzed for mean pore diameter, pore diameter distribution, and pore roundness distribution based on the procedure introduced in [23]. A MATLAB code was used for analyzing SEM raw images with first applying median filtering [24] to smoothen out high frequency noise. The filtered images were then segmented processed [25] by thresholding based on Otsu method [26] in order to convert the gray level images into binary black and white images. Thus, all carbon fibers became black and empty pores of GDL became white. Finally, the black and white images were gap filled to remove small gaps in the fibers and the pores. In order to make gap filling step more accurate, pore diameters less than 5μm were filtered out in our analysis. Figure 1 shows the four steps of image processing used in this study.

RESULTS AND DISCUSSION

SEM images were processed for microstructural analysis. Analysis includes mean pore diameter, pore diameter distribution and pore roundness distribution for different GDL samples used. Other than conducting a case by case comparison for GDLs of different thicknesses and for treated and untreated sample, pore diameter distribution for one untreated GDL sample (TGP_120) and at three different locations was also obtained as will be discussed in "In-Plane Pore Distribution" section. These distribution plots may be used to define the order of anisotropicity of GDLs in future studies but no quantitative analysis were done on them in this study. Finally, as mentioned in EXPERIMENTAL section, SEM images were processed based on Otsu method for threshold setting. In order to examine the validity of the results obtained based on this approach, the effect of threshold setting on mean pore diameter was also studied. Before all these microstructural analysis, liquid water droplet contact angle on GDLs were measured. Contact angle is a macro-scale property that represents the wetting ability of a solid surface by liquid. It is a function of interfacial energy along the three phase boundary. Measured contact angles can help illuminating the variation of GDL surface energy for different PTFE content within the GDL.

Contact Angle

Droplet contact angle describes solid surface interfacial tensions based on the Young's mechanical equilibrium relation. Liquid droplet contact angle on a solid surface like GDL introduces mechanical equilibrium of the droplet under the influence of three phase interfacial tensions [29]. Furthermore, droplet contact angle on GDL surface is one of the most important parameters in water management with application in PEFC since it directly affects some major properties with dominant effects on liquid water transport within and on GDL surface. Surface adhesion force (given in Eqn. 1), drag force from shear gas flow in gas channel (given in Eqn. 2), the capillary pressure and even droplet shape on GDL surface are some properties contact angle directly affects. Surface adhesion force keeps the droplet on GDL surface:

$$F_s = 2\sigma_{lv} d_d \sin^2\theta \sin(\Delta\theta) \tag{1}$$

where σ_{lv} is the surface tension between liquid and vapor, d_d is the diameter of a droplet upon detachment, θ is the contact angle and $\Delta\theta$ is the difference between advancing and receding contact angle [5]. Drag force tries to detach the droplet from the GDL surface:

$$F_D = \frac{1}{2}\rho C_D A_P V^2 \tag{2}$$

where ρ is the density of the gas flowing in the gas channel, C_D is the drag coefficient, A_P is the droplet projected area perpendicular to the gas flow and V is the superficial gas velocity.

Static contact angles measured in this study for each GDL sample is shown in Figure 2. Error bars shown represent the standard deviation calculated for each contact angle data point. It can be observed that droplet contact angle significantly changes from an untreated to a treated GDL surface while adding more amount of PTFE does not make any change on the contact angle. Furthermore, it seems that the GDL thickness does not affect the droplet contact angle. As Whitesides and Laibinis [30] reported, droplet behavior on GDL surface is mostly controlled by the wetting characteristics of the top few monolayers of the surface. That is why the thickness of the GDL shows no contribution to the droplet contact angle. Table 2 lists the mean contact angle measured for ten droplets being dropped on GDLs as well as the standard deviation calculated. For each GDL thickness, droplet contact angles on untreated GDL and treated GDLs with different amount of PTFE are shown. It can be concluded from Table 2 and Figure 2 that the average contact angle droplets make is about 150° on treated GDLs no matter the PTFE content and as mentioned earlier, the GDL thickness has no effect on this contact angle. Similar contact angle on GDLs with different PTFE contents has been observed and reported by other groups such as Fairweather et al. [31] and Benziger et al. [32]. It also lead us to draw a conclusion that PTFE particles mostly penetrate through the GDL and agglomerate within the GDL rather than sitting on its surface.

Mean Pore Diameter

GDLs mean pore diameters were obtained by analyzing SEM images based on the procedure introduced by Parikh et

TABLE 1: PROPERTIES OF GDLs USED IN THIS STUDY

Toray Carbon Paper Type	Manufacturer Specified GDL Thickness (μm)	GDL Thickness Measured (μm)	Manufacturer Specified Porosity	Bulk Density g cm^{-3}	Fiber Diameter μm	Air Permeability (m^2)	Areal Mass (mg cm^{-2})	PTFE Concentration in Emulsion (wt.%)
TGP-030	110	103	80%	-	-	-	4.7	10.4 wt.%
TGP-060	190	179	76% (78% [19,27])	0.44 [19]	-	-	8.6	10.3 wt.%
TGP-090	280	282	78% (80% [28])	0.45 [19]	9.2 [28]	8.9×10^{-12} [28]	12.6	10.5 wt.%
TGP-120	370	336	78%	0.45 [19]	-	8.7×10^{-12} [8]	16.5	10.4 wt.%

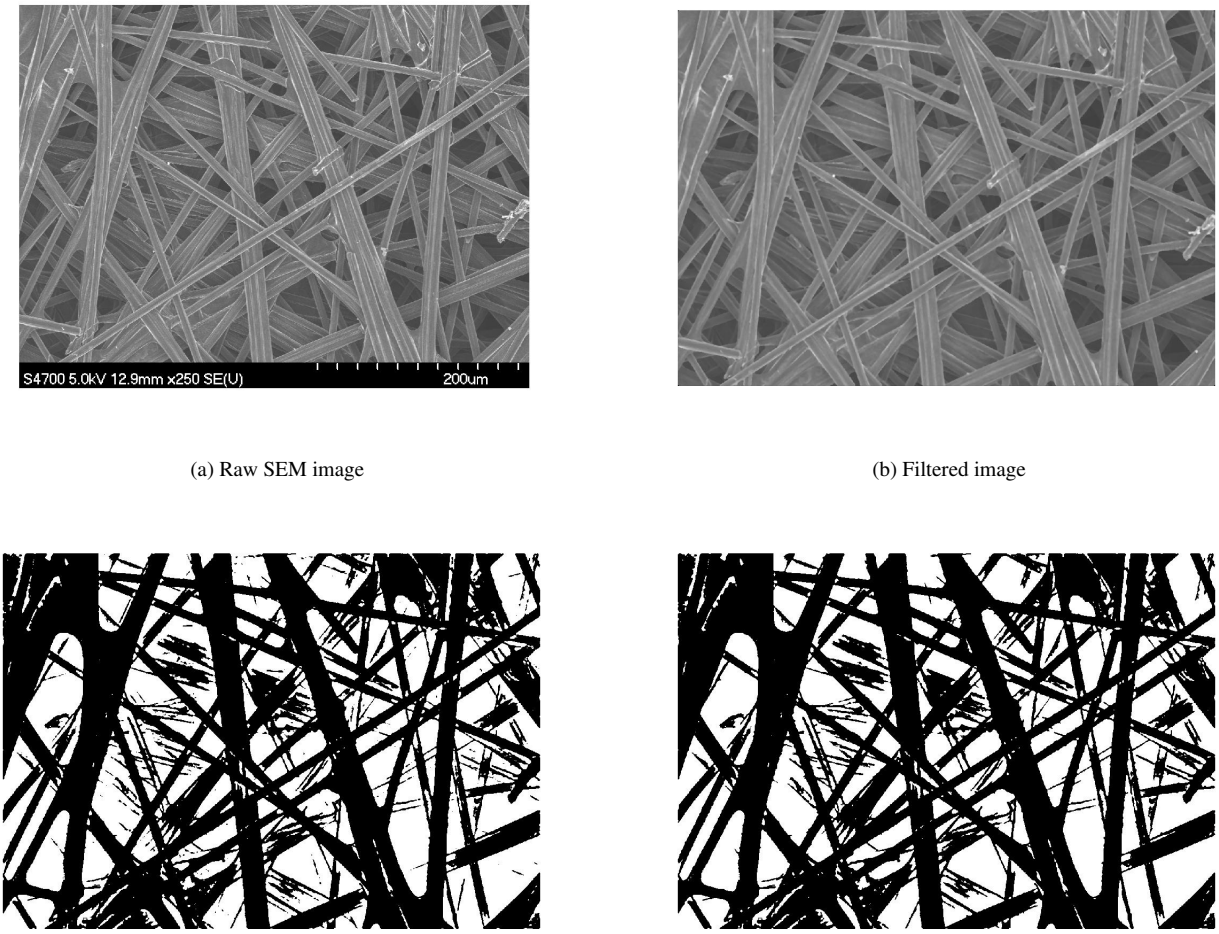

(a) Raw SEM image

(b) Filtered image

(c) Binary black and white image

(d) Gap filled black and white image

FIGURE 1: SEM IMAGE PROCESSING STEPS

al. [23]. For each GDL case, five SEM images were obtained with scan size of $507\mu\text{m} \times 356\mu\text{m}$ defined by ImageJ software developed by National Institute of Health. The overall mean pore diameter was calculated by averaging mean pore diameters obtained for each SEM image. GDL pore diameter is characterized by *equivalent pore diameter*, EPD, given by Eqn. 3:

TABLE 2: CONTACT ANGLE MEASURED FOR GDLs WITH DIFFERENT THICKNESSES

GDL Type	GDL Thickness (μm)	Contact Angle (°) (Untreated GDL)	Contact Angle (°) (PTFE content level #1)	Contact Angle(°) (PTFE content level #2)	Contact Angle(°) (PTFE content level #3)	Contact Angle(°) (PTFE content level #4)
TGP-030	110	$142.0° \pm 3.1°$	$153.9° \pm 2.4°$ (10 wt.%)	$150.9° \pm 1.7°$ (25 wt.%)	$150.2° \pm 4.3°$ (37 wt.%)	$147.8° \pm 2.5°$ (50 wt.%)
TGP-060	190	$129.7° \pm 8.8°$	$153.7° \pm 2°$ (10 wt.%)	$152.8° \pm 3°$ (25 wt.%)	$151.7° \pm 3°$ (35 wt.%)	$153.5° \pm 2°$ (55 wt.%)
TGP-090	280	$137.4° \pm 4.3°$	$156.4° \pm 1.5°$ (10 wt.%)	$153.6° \pm 2°$ (15 wt.%)	$149° \pm 2°$ (35 wt.%)	$154.9° \pm 1.5°$ (45 wt.%)
TGP-120	370	$141.3° \pm 5.0°$	$151.2° \pm 2.9°$ (10 wt.%)	$151.4° \pm 3.7°$ (15 wt.%)	$151.9° \pm 2.4°$ (30 wt.%)	NA

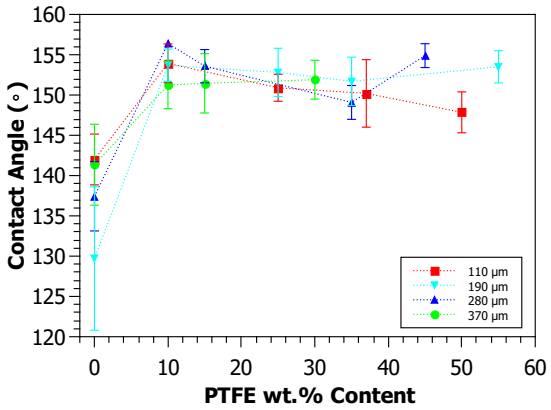

FIGURE 2: DROPLET CONTACT ANGLE ON TREATED AND UNTREATED GDLs

$$EPD = 2\sqrt{A/\pi} \tag{3}$$

where A is the area of the pore [33].

GDL pore size is one of the most important parameters in liquid water transport from catalyst layer, where water is produced as one of the byproducts of electrochemical reaction, to gas channel, where it can be drained either by detachment caused by shear gas flow or corner flow across the edges of the gas channels [5]. Liquid water passes through the GDL pores when its pressure exceeds the capillary pressure, and for a continuous flow, its pressure should remain higher than the capillary pressure [16]. Capillary pressure is defined as the difference between the pressure of liquid and gas phase at equilibrium ($P_c = P_l - P_g$) and is a function of mean curvature of water-air interface, contact angle and surface energy:

$$P_c = \frac{2\sigma_{\text{water}} \cos\theta}{\text{r}_{\text{pore}}} \tag{4}$$

where σ_{water} is interfacial surface tension, θ is the contact angle and r_{pore} is the pore radius. The smaller the pore radius, the greater the capillary pressure liquid water should overcome to be able to pass through the GDL. Tamayol and Bahrami [19] modeled GDL as a network of pores connected by throats. Based on their model, it is assumed that air and liquid water are stored in the pores and the the volume occupied by throats is negligible. Only throats resist liquid water transport and pores do not make any resistance to the flow [34]. It was reported that the capillary pressure increases with Toray carbon paper thickness [19]. Based on the model argued in [19], as the thickness of the GDL increases, the number of layers forming the GDL also increases. This directly increases the breakthrough pressure of the liquid water. Table 3 lists the mean pore diameter calculated for GDLs of different thicknesses. Based on the results obtained by this approach, GDL mean pore diameter is not changing with GDL thickness and even the mean pore diameter for untreated and treated GDLs are the same. The mean pore diameter obtained for all GDLs is about 26μm which is in well agreement with the mean pore diameter reported by Parikh et al. [23] for Toray carbon paper. The mean pore size given in [8,35] is within the range of $30-40\mu$m that is again in agreement with the results obtained in this work.

TABLE 3: MEAN PORE DIAMETER OF GDLs WITH DIFFERENT THICKNESSES

Toray Carbon Paper Type	GDL Thickness (μm)	Untreated GDL Mean Pore Diameter (μm)	10 wt.% Treated GDL Mean Pore Diameter (μm)
TGP-030	110	25.23 ± 0.47	25.46 ± 0.86
TGP-060	190	25.95 ± 0.66	26.94 ± 2.27
TGP-090	280	27.68 ± 1.05	26.49 ± 3
TGP-120	370	25.45 ± 0.22	NA

Considering average pore diameter of 26μm, average contact angle of 150° and water surface tension of 0.072Nm^{-1}, the capillary pressure will be calculated at 9.5kPa based on Eqn. 4. This pressure is almost twice as much as the breakthrough pressure reported in [36]. The reason behind is that for a mean pore

diameter of 26μm, there are some pores with larger diameter in the GDLs that result in lower capillary pressure, and as Bazylak et al. [37] had reported, liquid water chooses the path of least resistance through the GDL and emerge from the surface of the GDL in the form of droplet. Further discussion about pore diameter distribution will be given in next section. Figure 3 shows the calculated mean pore diameter as a function of GDL thickness both for treated and untreated GDL. As mentioned earlier, mean pore diameter does not change neither with GDL thickness nor with PTFE content within the GDL. PTFE particles are within the range of $50-500$nm [38] that is much smaller than the mean pore diameter.

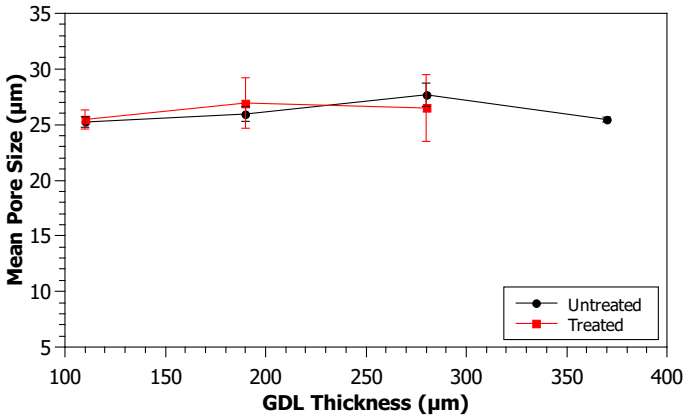

FIGURE 3: GDL MEAN PORE SIZE AS A FUNCTION OF ITS THICKNESS

Figure 3 and Table 3 also show higher standard deviation of mean pore diameter for treated GDLs compared to untreated ones. SEM images of treated GDL surface are shown in Figure 4. As shown on the Figure 4, the white areas between carbon fibers are PTFE emulsion dried on the surface of the GDL. Figure 4 shows even for the same GDL sample PTFE is not uniformly distributed and there can be some areas with higher PTFE content (Figure 4b) and some areas with lower PTFE content (Figure 4d). Other than uneven PTFE distribution in the plane of the GDL, Figure 4 shows PTFE emulsion mostly covers top layers of the GDL and it seems from the Figure that PTFE hardly penetrates into the GDL. Same observation has been reported by Lim and Wang [39] when they took SEM images of carbon papers treated with fluorinated ethylene propylene (FEP). However, this observation is in discrepancy with the conclusion drawn from contact angle measurement. PTFE distribution through the GDL will be further studied by the authors. Rofaiel et al. [38] had measured heterogeneous through-plane PTFE distribution in carbon papers by using SEM energy dispersive X-ray spectrometry (EDS) and detected larger concentration of fluorine (as PTFE's high concentration element) along the surface fibers and less fluorine in the central region of the GDL. Fishman et al. [40] measured through-plane porosity distribution of GDLs and concluded that PTFE accumulates at local minima near the surface of the paper GDLs. The SEM images taken for this study, however, cannot be used for PTFE through-plane distribution analysis.

Pore Diameter Distribution

Pore diameter distributions were obtained from the MATLAB code and are shown in Figure 5 for each GDL sample. It can be concluded that for both treated and untreated GDLs, the majority of pores have diameters of less than 20μm. However, the existence of larger pores mitigate liquid water transport through the GDL by lowering the capillary pressure required for intrusion. Furthermore, pore diameter distributions show the thinnest GDL (TGP_030) has more number of pores compared to other two GDLs. This can be interpreted as the thinnest GDL is more porous compared to other samples. This result is in well agreement with the manufacturer specified porosity values given in Table 1 although the difference is minor. Pore size distribution could also be obtained by using mercury intrusion porosimetery (MIP) [27,41]. In such technique, mercury as a non-wetting fluid on most surfaces is penetrated into the pores of GDL by applying pressure. The pressure applied is a function of pore diameter. Williams et al. [1] used this approach and obtained pore size distribution for E-TEK carbon paper, E-TEK carbon cloth and SGL carbon paper.

In-Plane Variation of Pore Diameter Distribution

Pore diameter distribution for one GDL and at three random locations on its surface is also studied in this work. Figure 6 shows the pore diameter distribution for three different locations on the untreated thickest GDL (TGP_120). Although the mean pore calculated for all three cases is about 25μm, the number of pores detected within each range of diameters are different. Again, it can be observed that the majority of pores detected have diameters of less than 20μm while there are larger pores detected in all thee locations.

Pore Roundness Distribution

Pore roundness, S, is a property that describes the shape of the pores and is defined by Eqn. 5:

$$S = 4\pi A/P^2 \tag{5}$$

where A is the pore area and P is the perimeter of the pore. For a perfect circle, pore roundness is 1 and as the roundness of the

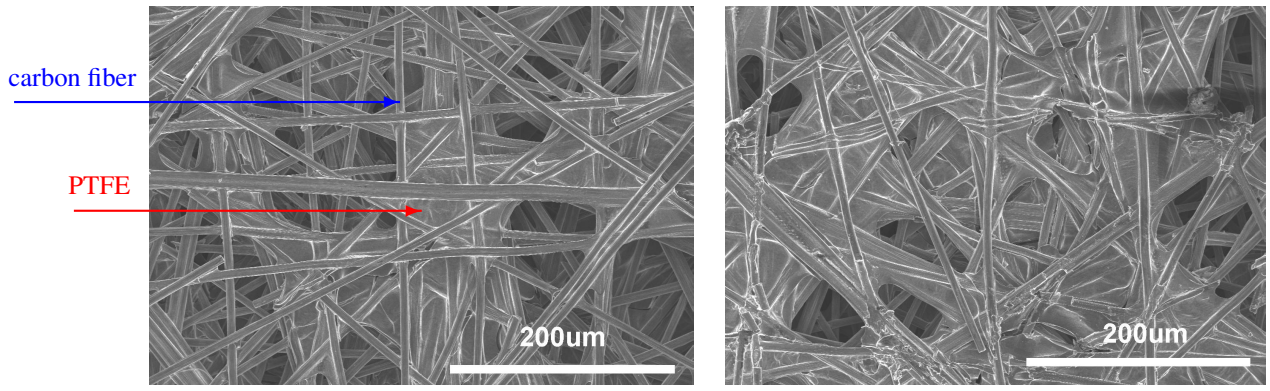

(a) Scan area 1

(b) Scan area 2

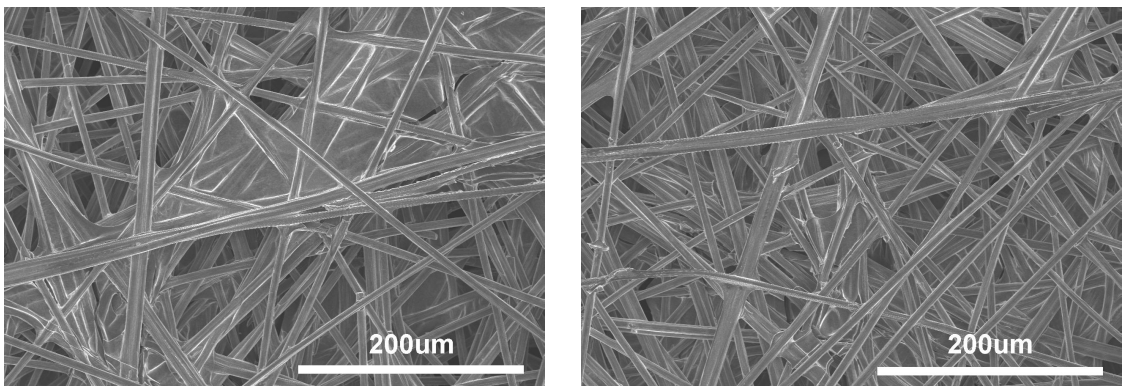

(c) Scan area 3

(d) Scan area 4

FIGURE 4: SEM IMAGE OF DIFFERENT LOCATIONS ON A TREATED GDL SAMPLE

shape decreases, this value also decrease. Pore roundness distribution of GDLs with different thicknesses are given in Figure 7. In general, no specific trend can be detected based on these histograms. It may be concluded that Toray carbon paper pores are mostly in random shape and don't follow any specific trend of a shape.

Effect of Threshold on Mean Pore Diameter

The MATLAB code processes the SEM images by converting gray level images into binary based on Otsu method. Threshold changes the degree of black and white objects in the image and can change the results obtained from images. In this section the effect of threshold setting on the mean pore diameter is studied. Figure 8 shows the variation of mean pore diameter as a function of threshold for TGP_060 GDL. The threshold defined based on Otsu method for this image was 0.3875. MATLAB code was ran to obtain the mean pore diameter for different thresholds starting from 0.35 with steps of 0.0125. Figure 8 shows negligible variation of mean pore diameter for different threshold settings. This strengthens the validity of the results obtained based on this approach.

CONCLUSION

GDL microstructural surface properties for different GDL thicknesses and for PTFE treated and untreated cases have been studied based on SEM images obtained. Consequent steps of image processing have been taken and SEM images were analyzed for mean pore diameter, pore diameter distribution and pore roundness as microstructural properties of the GDL. Droplet static contact angle on GDLs, as a macroscale surface property, has been measured using a setup made for this purpose. The following conclusions can be drawn from this study:

1. GDL thickness was observed to have no effect on droplet contact angle.
2. While droplet contact angles significantly increased from an untreated GDL to a PTFE treated one, the amount of PTFE content in GDL was observed to have no impact on the con-

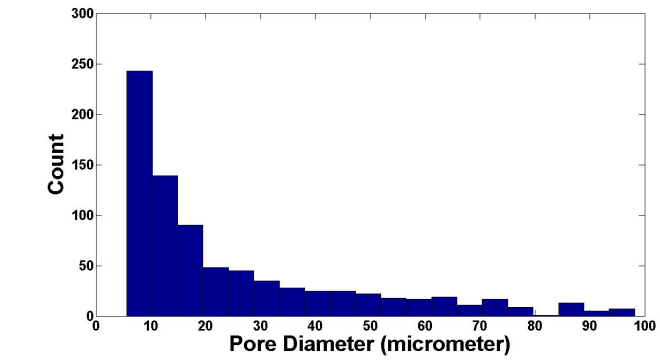

(a) Untreated GDL, TGP_030, (110μm)

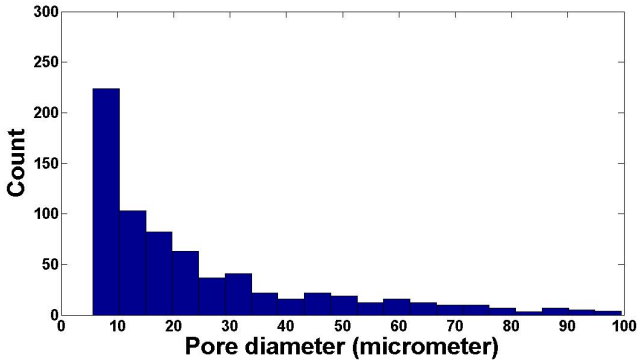

(b) Treated GDL, TGP_030, (110μm)

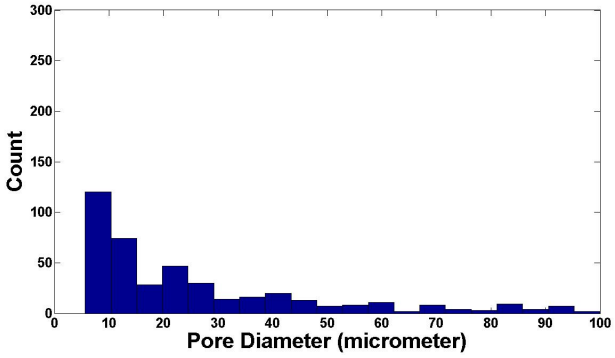

(c) Unreated GDL, TGP_060, (190μm)

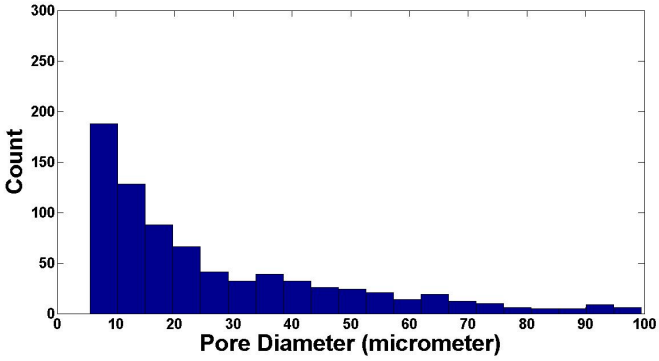

(d) Treated GDL, TGP_060, (190μm)

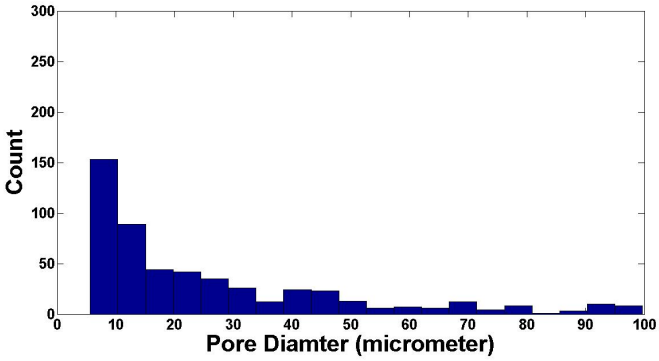

(e) Unreated GDL, TGP_090, (280μm)

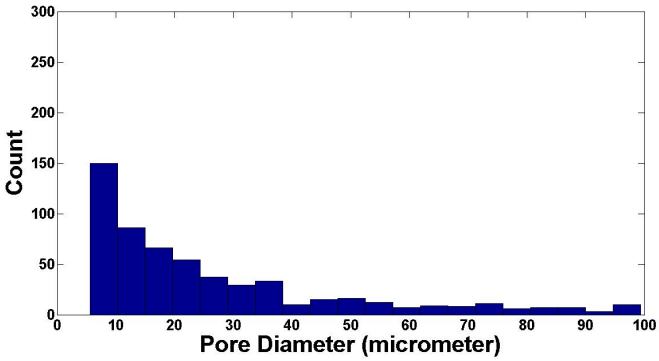

(f) Treated GDL, TGP_090, (280μm)

FIGURE 5: PORE DIAMETER DISTRIBUTION FOR GDLs OF DIFFERENT THICKNESSES

tact angles measured.

3. GDL mean pore diameter does not change with its thickness. Furthermore, mean pore diameter was observed to be the same for untreated and treated GDLs. Using SEM image, the mean pore diameter was analyzed to be around 26μm for treated and untreated Toray carbon papers of different thicknesses used.
4. The standard deviation of the mean pore diameter calculated for untreated GDLs were smaller than for untreated GDLs.
5. The PTFE loading approach taken in this study resulted in an uneven PTFE distribution on GDL surface (in-plane).
6. Threshold value in the range of the threshold defined by Otsu

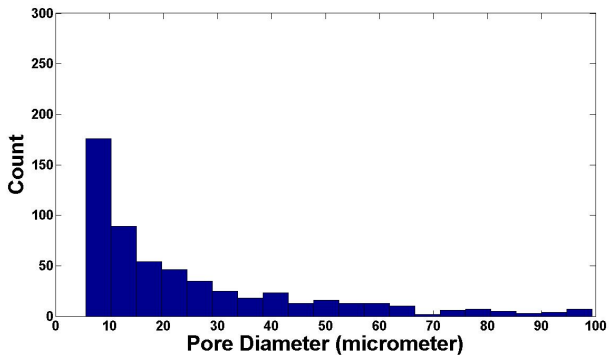

(a) location 1, mean pore diameter 25.3μm

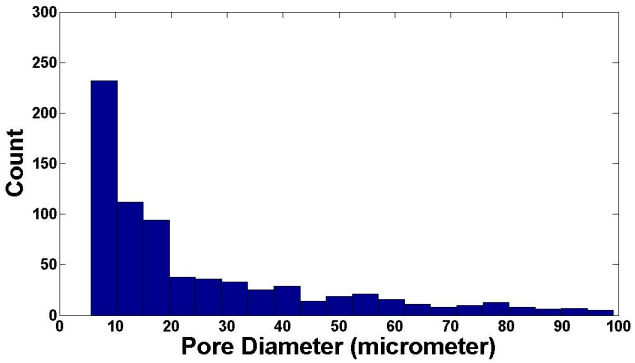

(b) location 2, mean pore diameter 25.7μm

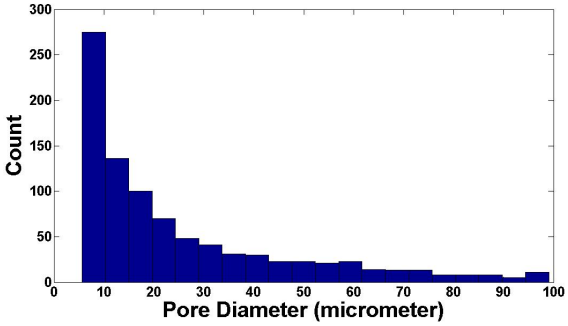

(c) location 3, mean pore diameter 25.35μm

FIGURE 6: PORE DIAMETER DISTRIBUTION FOR THREE RANDOM LOCATIONS ON UNTREATED TGP_120

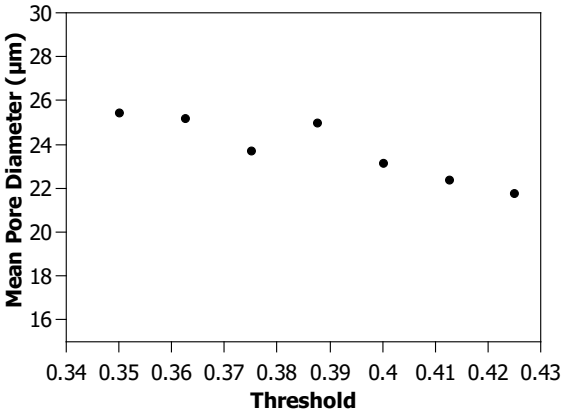

FIGURE 8: THE VARIATION OF CALCULATED MEAN PORE DIAMETER AS A FUNCTION OF THRESHOLD FOR TGP_060

method was observed to have negligible effect on mean pore diameter.

7. Pore diameter distribution plots indicate that the majority of pores fall within less than 20μm pore diameter.
8. Pore roundness distribution plots suggest a non attributable shape of Toray carbon paper pores.

ACKNOWLEDGMENT

Michigan Technological University is gratefully acknowledged for providing the startup fund for this research. The authors would like to thank Nishith Parikh from *Energy and Nano Science (ENS) Laboratory* at Michigan Technological University for taking SEM images and providing MATLAB code for SEM image analysis. Vinaykumar Konduru from *Microfluidic and Interfacial Transport Laboratory* [21] at Michigan Technological University is also appreciated for measuring the contact angles of droplets on GDLs.

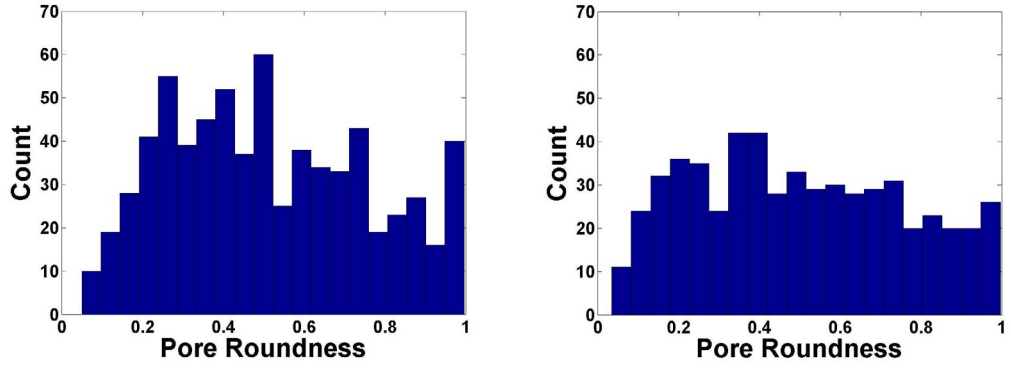

(a) Untreated GDL, TGP_030, (110μm)

(b) Treated GDL, TGP_030, (110μm)

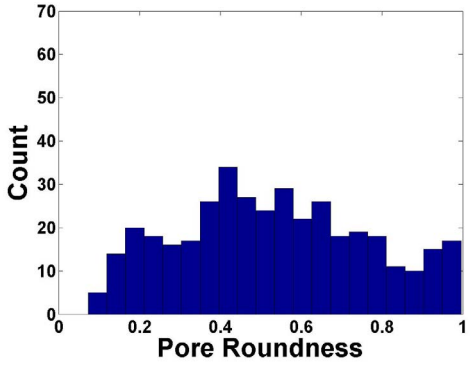

(c) Unreated GDL, TGP_060, (190μm)

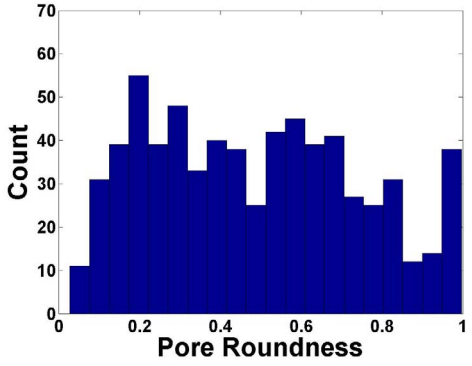

(d) Treated GDL, TGP_060, (190μm)

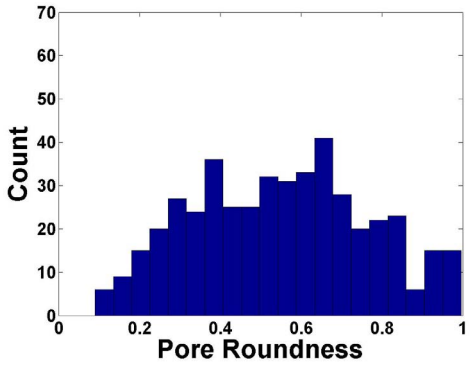

(e) Unreated GDL, TGP_090, (280μm)

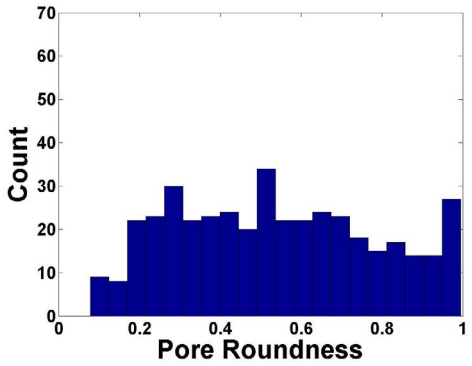

(f) Treated GDL, TGP_090, (280μm)

FIGURE 7: PORE ROUNDNESS DISTRIBUTION OF GDLs

REFERENCES

[1] M.V. Williams, E. Begg, L. Bonville, H.R. Kunz, J.M. Fenton, 2004. "Characterization of gas diffusion layers for PEMFC". *J. Electrochem. Soc.,* ***151***, p. A1173.

[2] T.V. Nguyen, 2006. "Water Management by Material Design and Engineering for PEM Fuel Cells". *ECS Transactions,* ***3***, pp. 1171–1180.

[3] P.K. Sinha, P.P. Mukherjee, C.Y. Wang, 2007. "Impact of GDL structure and wettability on water management in polymer electrolyte fuel cells". *J. Mater. Chem.,* ***17***(30), pp. 3089–3103.

[4] A. Bazylak, 2009. "Liquid water visualization in PEM fuel

cells: A review". *Int. J. Hydrogen Energy,* ***34***(9), pp. 3845–3857.

[5] F.Y. Zhang, X.G. Yang, C.Y. Wang, 2006. "Liquid Water Removal From A Polymer Electrolyte Fuel Cell". *J. Electrochem. Soc.,* ***153***, p. A225.

[6] W. Dai, H. Wang, Z.Z. Yuan, J.J. Martin, D. Yang, J. Qiao, J. Ma, 2009. "A review on water balance in the membrane electrode assembly of proton exchange membrane fuel cells". *Int. J. Hydrogen Energy,* ***34***(23), pp. 9461–9478.

[7] K. Tüber, D. Pócza, C. Hebling, 2003. "Visualization of water buildup in the cathode of a transparent PEM fuel cell". *J. Power Sources,* ***124***(2), pp. 403–414.

[8] D. Spernjak, A.K. Prasad, S.G. Advani, 2007. "Experimental investigation of liquid water formation and transport in a transparent single-serpentine PEM fuel cell". *J. Power Sources,* ***170***, pp. 334–344.

[9] X.G. Yang, F.Y. Zhang, A.L. Lubawy, C.Y. Wang, 2004. "Visualization of liquid water transport in a PEFC". *Electrochem. Solid St.,* ***7***, p. A408.

[10] A. Theodorakakos, T. Ous, M. Gavaises, J.M. Nouri, N. Nikolopoulos, H. Yanagihara, 2006. "Dynamics of water droplets detached from porous surfaces of relevance to PEM fuel cells". *J. Colloid Interf. Sci.,* ***300***(2), pp. 673–687.

[11] M.A. Hickner, N.P. Siegel, K.S. Chen, D.S. Hussey, D.L. Jacobson, M. Arif, 2008. "In Situ High-Resolution Neutron Radiography of Cross-Sectional Liquid Water Profiles in Proton Exchange Membrane Fuel Cells". *J. Electrochem. Soc.,* ***155***, p. B427.

[12] A.M. Niroumand, M. Saif, 2010. "Two-phase flow measurement system for polymer electrolyte fuel cells". *J. Power Sources,* ***195***(10), pp. 3250–3255.

[13] G. Lin, T.V. Nguyen, 2005. "Effect of Thickness and Hydrophobic Polymer Content of the Gas Diffusion Layer on Electrode Flooding Level in a PEMFC". *J. Electrochem. Soc.,* ***152***, pp. A1942–A1948.

[14] G.G. Park, Y.J. Sohn, T.H. Yang, Y.G. Yoon, W.Y. Lee, C.S. Kim, 2004. "Effect of PTFE contents in the gas diffusion media on the performance of PEMFC". *J. Power Sources,* ***131***, pp. 182–187.

[15] U. Pasaogullari, C.Y. Wang, 2004. "Liquid Water Transport in Gas Diffusion Layer of Polymer Electrolyte Fuel Cells". *J. Electrochem. Soc.,* ***151***, p. A399.

[16] J.H. Nam, M. Kaviany, 2003. "Effective diffusivity and water-saturation distribution in single-and two-layer PEMFC diffusion medium". *Int. J. Heat Mass Tran.,* ***46***(24), pp. 4595–4611.

[17] S. Litster, D. Sinton, N. Djilali, 2006. "Ex situ visualization of liquid water transport in PEM fuel cell gas diffusion layers". *J. Power Sources,* ***154***(1), pp. 95–105.

[18] R. Defay, I. Prigogine, 1966. *Surface tension and adsorption*. Wiley.

[19] A. Tamayol, M. Bahrami, 2011. "Water permeation through gas diffusion layers of proton exchange membrane fuel cells". *J. Power Sources*.

[20] C.M. Hwang, M. Ishida, H. Ito, T. Maeda, A. Nakano, Y. Hasegawa, N. Yokoi, A. Kato, T. Yoshida, 2010. "Influence of properties of gas diffusion layers on the performance of polymer electrolyte-based unitized reversible fuel cells". *Int. J. Hydrogen Energy,* ***36***, p. 1740.

[21] http://www.me.mtu.edu/mnit/.

[22] V. Konduru, 2010. "Static and Dynamic Contact Angle Measurement on Rough Surfaces Using Sessile Drop Profile Analysis with Application to Water Management in Low Temperature Fuel Cells". Master's thesis, Michigan Technological University.

[23] N. Parikh, J.S. Allen, R.S. Yassar. "Microstructure of Gas Diffusion Layers for PEM Fuel Cells". *Fuel Cells*.

[24] G. Leinhardt, and S. Leinhardt, 1980. "Exploratory data analysis: New tools for the analysis of empirical data". *Rev. Res. Educ.*, pp. 85–157.

[25] Sezgin, M., and Sankur, B., 2004. "Survey over image thresholding techniques and quantitative performance evaluation". *J. Eectron. Imaging,* ***13***(1), pp. 146–168.

[26] N. Otsu, 1975. "A threshold selection method from gray-level histograms". *Automatica,* ***11***(285-296), pp. 23–27.

[27] J.T. Gostick, M.A. Ioannidis, M.W. Fowler, M.D. Pritzker, 2009. "Wettability and capillary behavior of fibrous gas diffusion media for polymer electrolyte membrane fuel cells". *J. Power Sources,* ***194***(1), pp. 433–444.

[28] J.T. Gostick, M.W. Fowler, M.D. Pritzker, M.A. Ioannidis, L.M. Behra, 2006. "In-plane and through-plane gas permeability of carbon fiber electrode backing layers". *J. Power sources,* ***162***(1), pp. 228–238.

[29] E.C. Kumbur, K.V. Sharp, M.M. Mench, 2006. "Liquid droplet behavior and instability in a polymer electrolyte fuel cell flow channel". *J. Power Sources,* ***161***(1), pp. 333–345.

[30] G.M. Whitesides, P.E. Laibinis, 1990. "Wet chemical approaches to the characterization of organic surfaces: self-assembled monolayers, wetting, and the physical-organic chemistry of the solid-liquid interface". *Langmuir,* ***6***(1), pp. 87–96.

[31] J.D. Fairweather, P. Cheung, D.T. Schwartz, 2010. "The effects of wetproofing on the capillary properties of proton exchange membrane fuel cell gas diffusion layers". *J. Power Sources,* ***195***(3), pp. 787–793.

[32] J. Benziger, J. Nehlsen, D. Blackwell, T. Brennan, J. Itescu, 2005. "Water flow in the gas diffusion layer of PEM fuel cells". *J. Membr. Sci.,* ***261***(1-2), pp. 98–106.

[33] B.R. Jennings, K. Parslow, B.R. Jennings, K. Parslow, 1988. "Particle size measurement: the equivalent spherical diameter". *Pro. Roy. Soc. London. A. Mathematical and*

Physical Sciences, ***419***(1856), pp. 137–149.
[34] F.A.L. Dullien, Porous Media: Fluid Transport and Pore Structure, 2nd ed., Academic Press, New York, 1992.
[35] J. Ihonen, M. Mikkola, and G. Lindbergh, 2004. "Flooding of Gas Diffusion Backing in PEFCs, Physical and Electrochemical Characterization". *J. Electrochem. Soc.,* ***151***(8), pp. A1152–A1161.
[36] T.L. Liu, C. Pan, 2012. "Visualization and back pressure analysis of water transport through gas diffusion layers of proton exchange membrane fuel cell". *J. Power Sources*.
[37] A. Bazylak, D. Sinton, N. Djilali, 2008. "Dynamic water transport and droplet emergence in PEMFC gas diffusion layers". *J. Power Sources,* ***176***(1), pp. 240–246.
[38] A. Rofaiel, J.S. Ellis, P.R. Challa, A. Bazylak, 2012. "Heterogeneous through-plane distributions of polytetrafluoroethylene in polymer electrolyte membrane fuel cell gas diffusion layers". *J. Power Sources,* ***201***, pp. 219–225.
[39] C. Lim, C.Y. Wang, 2004. "Effects of hydrophobic polymer content in GDL on power performance of a PEM fuel cell". *Electrochim. Acta,* ***49***(24), pp. 4149–4156.
[40] Z. Fishman and A. Bazylak, 2011. "Heterogeneous Through-Plane Porosity Distributions for Treated PEMFC GDLs I. PTFE Effect". *J. Electrochem. Soc.,* ***158***, p. B841.
[41] K.G. Gallagher, R.M. Darling, T.W. Patterson, M.L. Perry, 2008. "Capillary Pressure Saturation Relations for PEM Fuel Cell Gas Diffusion Layers". *J. Electrochem. Soc.,* ***155***, p. B1225.